Response Error Correction—A Demonstration of Improved Human-Machine Performance Using Real-Time EEG Monitoring

Lucas C. Parra, Clay D. Spence, Adam D. Gerson, and Paul Sajda

***Abstract*—We describe a brain–computer interface (BCI) system, which uses a set of adaptive linear preprocessing and classification algorithms for single-trial detection of error related negativity (ERN). We use the detected ERN as an estimate of a subject's perceived error during an alternative forced choice visual discrimination task. The detected ERN is used to correct subject errors. Our initial results show average improvement in subject performance of 21% when errors are automatically corrected via the BCI. We are currently investigating the generalization of the overall approach to other tasks and stimulus paradigms.**

***Index Terms*—Brain–computer interface (BCI), electroencephalography (EEG), error related negativity (ERN), eye blink removal, single-trial detection.**

I. Adaptive Human–Computer Interface

The performance of a human subject executing a task while interacting with a computer can be highly variable, depending upon such individual factors as level of alertness, reaction speed, working memory capacity, and capacity to perform parallel tasks. Most current human–computer interfaces (HCI) do not adapt to the physiological or psychological state of the user. The goal of an *adaptive* interface is to estimate variables correlated with human performance and adapt the HCI accordingly (e.g., adjust speed of display, provide appropriate cues, automatically correct errors, etc.) Several behavioral and physiological measures, such as reaction time, eye motion, and pupil dilation, have been proposed as variables having utility for adapting an HCI [1], [2]. More recently, research in neuroimaging has identified electroencephalography (EEG) signals that are correlated with attention [3], memory encoding [4], motor imagery [5], perceived error and/or conflict [6], perception/recognition [7] and which, therefore, might be useful for such adaptation.

In this paper, we describe a brain–computer interface (BCI) capable of monitoring a subject's cognitive state associated with specific observable events. We argue that this information can be used to adapt the HCI, and ultimately maximize performance. As an example, we demonstrate our initial results using a high-throughput, alternative forced choice visual discrimination task. In this task, a subject discriminates between two visual stimuli by pressing one of two buttons. When subjects attempt to minimize their response time, they often commit errors that are perceived shortly after the button-push response.[1] Interestingly, such perceived errors are accompanied by a negative fronto-central deflection in the EEG signal. This signal is known as the error related negativity (ERN) [9]. Single-trial detection of the ERN has been proposed as a means of correcting communication errors in a BCI system [10]. For offline processing, we have recently reported (using a simple linear classifier) up to 79% correct detection of the ERN within 100 ms of the erroneous response [8].

In this paper, we describe a BCI system which uses the detected ERN to correct erroneous responses of subjects so as to minimize the overall human-machine error rate. In particular, we focus on a set of adaptive, linear algorithms for data preprocessing and ERN detection. The algorithms are designed for single-trial, online processing and run in real-time on data that is streaming from a 64-channel EEG system through Ethernet. The latency of the total system is approximately 230 ms which is primarily constrained by the 200 ms integration time required for ERN detection.

BCI systems are currently being developed primarily as a communications means for severely motor impaired subjects. We are currently exploring other applications of the proposed real-time monitoring. For instance, we argue that one may be able to increase the speed of visual search for image analysts by detecting the activity associated with fast visual recognition. Single-trial detection of this activity permits bypassing slow motor response, thereby increasing human performance as we have demonstrated in a rapid visual serial presentation (RSVP) paradigm [11].

II. Adaptive Linear On-Line Real-Time Processing

We describe in Sections II-A and B novel algorithms for EEG eye blink removal and denoising. These algorithms preserve the ERN signal and, in fact, improve detection accuracy as presented in Section II-C. In all cases, we first remove baseline drifts, most likely due to slow skin conductivity changes, by filtering each channel with a recursive linear high-pass filter (second-order Butterworth with 1-Hz cut-off frequency).

A. Robust Eye Blink Removal With Principal Component Analysis

The muscle activity of eye blinks generates strong electrical signals that are linearly superimposed with smaller magnitude signals of interest (e.g., the ERN). Here, we present a novel algorithm for eye blink removal. Conventional algorithms detect eye blinks to simply discard the corresponding segment of data. This is not feasible in practice given the frequent eye motion in most real-world situations. A better approach is to subtract the artifacts using linear regression algorithms (e.g., [12]). Existing methods typically use electrooculogram (EOG) electrodes as a reference. Unfortunately, in addition to eye motion, EOG signals also contain frontal cortical activity which should not be subtracted. We construct a better reference signal using a linear combination of all electrodes, thereby increasing the power of the eye blink activity in the reference.

Let $\mathbf{x}(t)$ be the observed EEG sensor reading, $y(t)$ be the eye blink signal, and $\mathbf{s}(t)$ be the remaining signal of interest

$$\mathbf{x}(t) = \mathbf{a}y(t) + \mathbf{s}(t). \tag{1}$$

The linear coupling of the eye blink source $y(t)$ with the EEG sensors is denoted as $\mathbf{a}$. The arbitrary scale in the factorization $\mathbf{a}y(t)$ can be constrained by setting $\mathbf{a}^T\mathbf{a} = 1$. Given $\mathbf{a}$, we can generate a new signal $\tilde{\mathbf{x}}(t)$, which only contains the signal of interest when the orientation of the eye blink is removed

$$\tilde{\mathbf{x}}(t) = (\mathbf{I} - \mathbf{a}\mathbf{a}^T)\mathbf{x}(t) = (\mathbf{I} - \mathbf{a}\mathbf{a}^T)\mathbf{s}(t). \tag{2}$$

Only source signals that are exactly collinear with $\mathbf{a}$ are removed. All other source signals will have at least a residual contribution to $\tilde{\mathbf{x}}(t)$ and may be detected with appropriate algorithms.

Manuscript received June 16, 2002; revised February 14, 2003. This work was supported by the Defense Advanced Research Projects Agency under the Augmented Cognition program of the Information Processing Technology Office.

L. C. Parra and C. D. Spence are with Sarnoff Corporation, Princeton, NJ 08540 USA (e-mail: lparra@sarnoff.com; cspence@sarnoff.com).

A. D. Gerson and P. Sajda are with the Department of Biomedical Engineering, Columbia University, New York, NY 10024 USA (e-mail: ps629@columbia.edu, adg71@columbia.edu).

Digital Object Identifier 10.1109/TNSRE.2003.814446

[1]For more detailed description of the experimental paradigm, see [8].

1534-4320/03$17.00 © 2003 IEEE

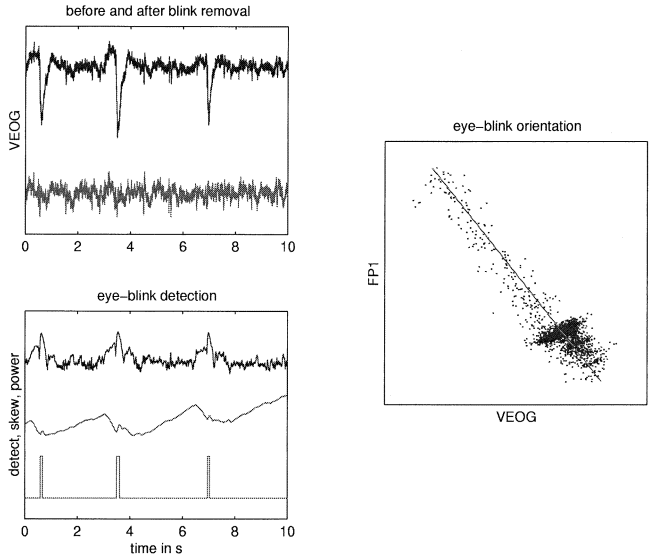

Fig. 1. Eye-blink detection and subtraction using first principal component. (top left) EOG channel before and after subtraction of eye blinks. (right) Scatter plot of the activity in EOG electrode and a frontal electrode during the same 10-s time interval. Solid line shows the orientation of the first principal component estimated during eye blinks. (bottom left) Power magnitude (upper trace) and time averaged skew (center trace) of the power in frontal and EOG electrodes, as well as eye blink detector output (lower trace).

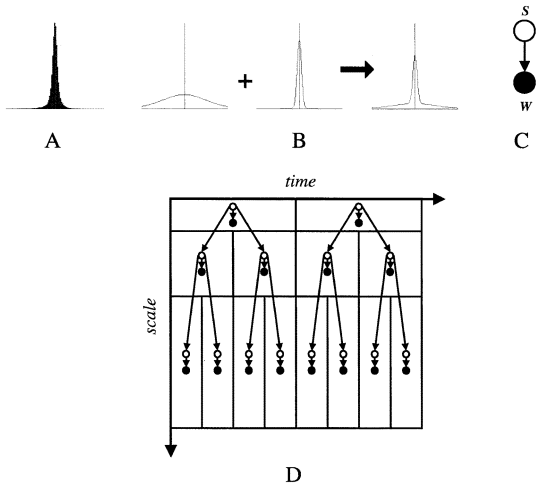

Fig. 2. Overview of the HMT. (A) Marginal distribution of evoked response EEG wavelet coefficients showing large peak and long tails (kurtosis = 17.5). (B) Two-state Gaussian mixture model for the marginal distribution of evoked response EEG. (C) Graphical representation of state dependencies on observed wavelet coefficients (white nodes are hidden variables, black nodes are observed). (D) Hidden Markov tree indicating the dependencies between scales.

The key challenge lies in estimating the coupling $\mathbf{a}$. Recent work suggests to use independent component analysis (ICA) in order to identify such linear projection associated with EEG artifacts [13]. In our experience, however, ICA methods have not proven robust when applied online. Fortunately, during eye blinks, the activity $y(t)$ is large compared to the signals of interest $\mathbf{s}(t)$. This is, in particular, true for frontal electrodes and EOG signals commonly acquired with EEG. The projection $\mathbf{a}$ can, therefore, be identified using principal component analysis (PCA) for which a number of robust online algorithms are available.

Our method partitions the 64 recorded channels into two sets: 1) the EOG and frontal electrodes containing strong eye blink signals and 2) the remaining parietal, temporal, and occipital electrodes with weaker eye blink signal contributions. Let us denote this partitioning with $\mathbf{x}(t) = [\mathbf{x}_1(t), \mathbf{x}_2(t)]$ and correspondingly $\mathbf{a} = [\mathbf{a}_1, \mathbf{a}_2]$. We propose to identify $\mathbf{a}_1$ as the first principal component of $\mathbf{x}_1(t)$ estimated *during eye blinks* as demonstrated in Fig. 1. Given the coupling $\mathbf{a}_1$, we obtain an estimate for the eye blink signal as, $\hat{y} = \mathbf{a}_1^T \mathbf{x}_1(t)$, since $\hat{y}(t) \approx y(t)$ for the case that $y(t) \ll \mathbf{a}^T \mathbf{s}$. The partitioning further weights the eye muscle activity in the estimate $\hat{y}$. The remaining coupling factors $\mathbf{a}_2$ can be determined with conventional regression, i.e., as the linear predictors of $\mathbf{x}_2$ given $\hat{y}(t)$. Interestingly, the update equations for the principal components $\mathbf{a}_1$, and the regression coefficients $\mathbf{a}_2$ have the same analytic form and can be combined into a single online update equation. After normalizing with the output power to accelerate convergence with a constant learning rate μ, the update becomes

$$\Delta \mathbf{a} = -\mu \left(\mathbf{a} - \frac{\mathbf{R}_{\mathbf{x}\mathbf{x}_1}(t)\mathbf{a}}{\mathbf{a}^T \mathbf{R}_{\mathbf{x}_1\mathbf{x}_1}(t)\mathbf{a}} \right) \tag{3}$$

where $\mathbf{R}_{\mathbf{x}\mathbf{x}_1}(t)$ and $\mathbf{R}_{\mathbf{x}_1\mathbf{x}_1}(t)$ are the corresponding portions of a running estimate of the covariance of $\mathbf{x}$ during eye blinks, e.g., $\mathbf{R}_{\mathbf{x}\mathbf{x}}(t) = \gamma \mathbf{R}_{\mathbf{x}\mathbf{x}}(t-1) + (1-\gamma)\mathbf{x}(t)\mathbf{x}_1^T(t)$ with a forgetting factor γ. For the required eye blink detection, we use the instantaneous magnitude, and a time-averaged skew of the power in $\mathbf{x}_1(t)$. A blink is detected when these quantities cross a predetermined threshold.

Fig. 1 shows a scatter plot of the signals of two electrodes in the set $\mathbf{x}_1$ and the corresponding orientations in $\mathbf{a}_1$ as they have been identified a few seconds after observing only a single blink. Eye blinks last for approximately 100 ms, which at 250-Hz sampling rate corresponds to about 25 samples to estimate $\mathbf{R}_{\mathbf{x}\mathbf{x}}(t)$. Only a few hundred iterations of (3) are required for convergence, i.e., 2–3 s after that eye blink. Subsequent eye blinks are accurately subtracted, as seen in Fig. 1. We find that $\mathbf{a}_1$ does not change much in the course of an experiment, and only a few eye blinks are required for an accurate estimation of the covariance matrixes. We can, therefore, set the detector thresholds and learning constant to very conservative values.

B. Denoising the ERN Using Temporal Hidden-Markov-Trees

One challenge in detecting the cognitive state of a subject via single-trial EEG is the inherently low signal-to-noise ratio (SNR). In developing denoising algorithms for improving the SNR, it is critical to obtain accurate noise estimates as well as exploit properties of the signal which preserve its structure. For the purpose of detection, noise is defined here as temporal activity in the EEG that is unrelated to the ERN. We, therefore, develop a statistical noise model using the activity during some unrelated baseline period. This model is then used to remove noise during the time period of the evoked response. We expect the wavelet transform of evoked potentials, as with many other types of natural signals [14], to exhibit the persistence of large or small coefficients across scale and the clustering of coefficients within scale. In addition, observations on the distribution of wavelet coefficients of EEG evoked potentials reveal that the coefficients have near zero mean and long tails—i.e., they are super-Gaussian [see Fig. 2(a)]. Here, we propose to estimate noise statistics by modeling such signal properties with a hierarchical probability model.

Super-Gaussian distributions may be approximated using a two-state zero-mean Gaussian mixture model in which the large number of small coefficients are modeled with a low-variance Gaussian and the small number of large coefficients are modeled with a high-variance Gaussian [Fig. 2(b)]. To efficiently describe the statistics of wavelet coefficients, each coefficient is associated with a hidden-state variable that describes whether the coefficient is in either a high- or low-variance state [Fig. 2(c)].

In order to model the conditional relationships described by persistence properties of wavelet coefficients, hidden-state variables are

linked across scales. Coefficients within scale are assumed to have the same probability density function, an approximation referred to as "tying" within scale. Fig. 2(d) shows the hidden Markov tree (HMT), which was first developed by Crouse *et al.* [14] and represents a graphical model of a set of dependencies between wavelet coefficients. The HMT, and similar models, have been used for a wide variety of signal and image processing applications including classification, segmentation, compression, synthesis, and denoising [15]–[18].

The parameters of the two-state zero-mean HMT consist of 1) the probability mass function p_i^S describing the high-/low-variance state of the wavelet coefficients of the coarsest scale, 2) the state transition matrices describing persistence between adjacent scales, and (3) the variances of the Gaussian mixture model, σ_L^2 and σ_H^2.

These parameters can be estimated using a modified Baum–Welch/upward-downward expectation maximization algorithm [19]. For the data shown in Fig. 3, we find that after training the transition matrices across scale are not uniformly distributed between states. This confirms the modeling assumption of the persistence of large or small coefficients across scale.

We follow the denoising methods outlined in [14]. Assume that the relationship between the wavelet coefficients of the observed EEG signal w_i^k, clean signal y_i^k, and noise n_i^k may be described as

$$w_i^k = y_i^k + n_i^k \tag{4}$$

where the subscript i indicates the ith wavelet coefficient and the superscript k indicates it comes from the kth wavelet tree. Assuming independent Gaussian white noise, we can estimate the state dependent clean signal variance $\sigma_{i,m}^2$ from the noisy signal variance $\gamma_{i,m}^2$

$$\sigma_{i,m}^2 = \left(\gamma_{i,m}^2 - \sigma_n^2\right)_+ \tag{5}$$

where m indicates the state and $(x)_+$ indicates a rectification allowing for only zero and positive values of its argument.[2] In the results, we present an estimate of noise variance is derived from the variance of the finest scale wavelet coefficients. However, this estimate can be adjusted to use only a specific subspace of the wavelet basis, depending upon prior knowledge of the noise source or interfering signal.

An estimate of the clean signal wavelet coefficients y_i^k, given the noisy wavelet coefficients and state variables is given by

$$E\left[Y_i^k | W_i^k = w_i^k, S_i^k = m\right] = \frac{\sigma_{i,m}^2}{\sigma_n^2 + \sigma_{i,m}^2} w_i^k. \tag{6}$$

Marginalizing over the state variable S_i^k results in

$$E\left[y_i^k | \mathbf{w}^k\right] = \sum_m p\left(S_i^k = m | \mathbf{w}^k\right) \times \frac{\sigma_{i,m}^2}{\sigma_n^2 + \sigma_{i,m}^2} w_i^k \tag{7}$$

where $\mathbf{w}^k$ is a vector representing all coefficients in the kth tree. Given these estimates for the clean signal wavelet coefficients, the inverse wavelet transform is applied to reconstruct the signal.

Examples of original and HMT denoised EEG signals, after eye blink removal, are demonstrated in Fig. 3 for a 10-s segment of data. For the single-trial analysis the HMT denoising is applied to a short segment of data of about 500 ms around the event of interest (button push). The HMT parameters are estimated for each channel from a single event at the beginning of the experiment.

C. ERN Detection With Linear Discriminant Analysis

We have previously reported [8] offline single trial detection of ERN, in a time window 0–100 ms following the button-push response, with an accuracy of $A_z = 0.79 \pm 0.05$ using a linear classifier on 64 electrodes.

[2]This rectification can cause deviation from linearity. However, in practice it is not a factor since the difference is almost always positive.

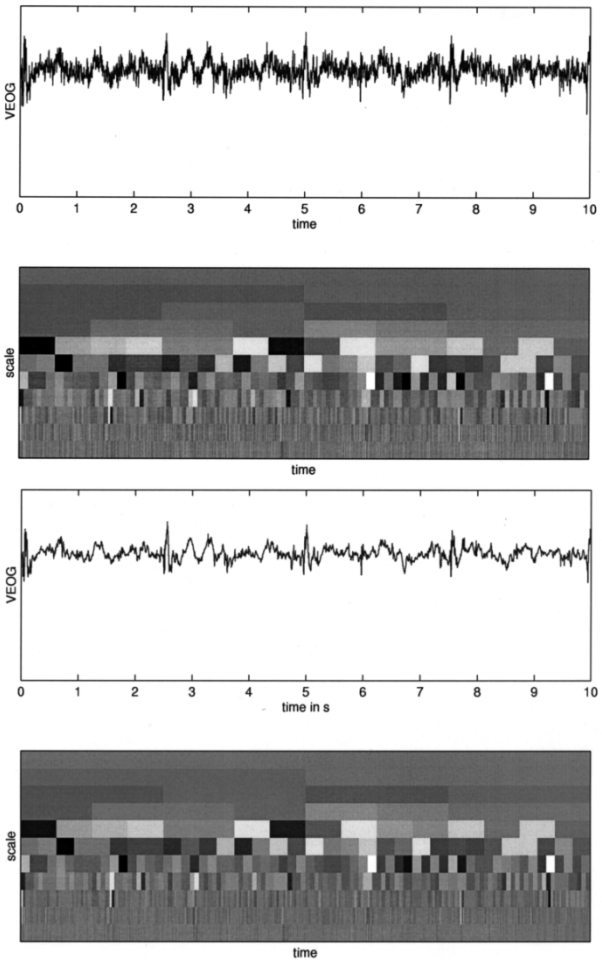

Fig. 3. Results of single-trial denoising using the HMT. (Top) original (noisy) signal after eye blink removal. (Bottom) clean signal denoised using HMT. Shown are the signals and wavelet decompositions.

In addition to the preprocessing methods just described, we have looked to improve detection accuracy by adding a second detection interval of 100 ms following the conventional time window of 0–100 ms after the response. The input to the linear classifier is a combination of two time windows of 64 leads (128 inputs). To improve classification and reduce the effect of high-frequency noise, we bootstrap the data by selecting multiple samples within a single trial as training data. At a 250-Hz sampling rate, the 200 ms following the response results in 25 training samples, each of dimension 128.

Our online detector is a Gaussian classifier and can be adapted by simply updating the mean and covariance estimates for the two classes using the most recent sample. With equal covariance for the two classes (errors/corrects), this results in linear classification. The advantage of linear classification is that we can compute the coupling of the discriminating source activity with the sensors. This provides a spatial map of the origin of the discriminating activity. The results obtained for a typical subject are shown in Fig. 4. The previously described fronto-central negativity is observed during the 100 ms following the response. In addition, a more prolonged bilateral posterior positivity is observed for correct trials, which further improves discrimination. The single-trial discrimination performance for the seven subjects analyzed in [8] increases to $A_z = 0.90 \pm 0.04$ when using offline linear preprocessing. Note the processing sequence: eye blink removal, followed by HMT

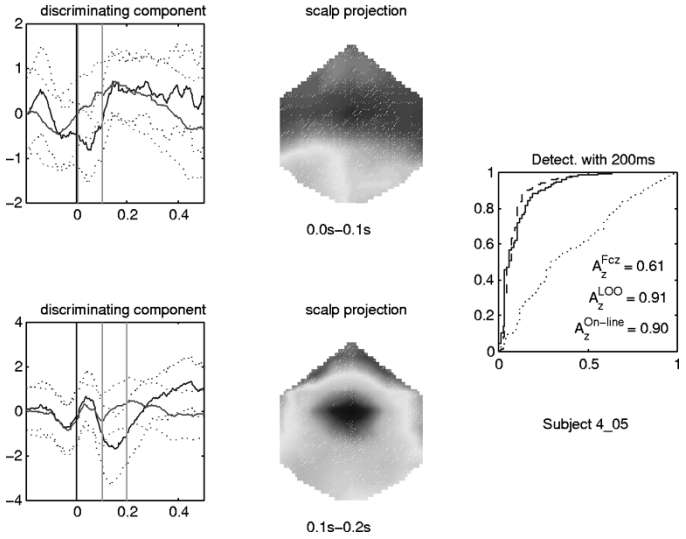

Fig. 4. ERN detection using linear discrimination combining the time intervals 0–100 ms and 100–200 ms after response. (left) Discriminating component and (center) scalp projection graphs results were obtained with offline linear classification. Similar results are obtained with online adaptation. (right) Single-trial ROC results compare A_z for offline (LOO), online and using only F_{cz} electrode. Note that on- and offline are comparable.

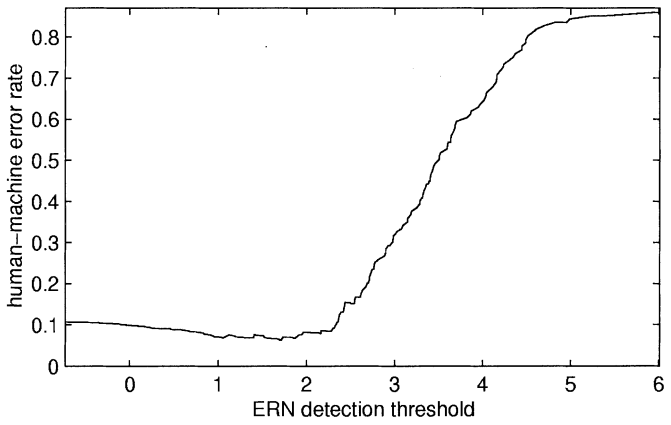

Fig. 5. Total human–machine performance after correcting human response errors based on ERN detection as a function of classifier threshold. Note that the minimum is not at zero, indicating that the underlying distributions deviate from Gaussian.

denoising, followed by linear classification. The largest jump in performance was due to the eye blink removal (A_z increases from 0.79 to 0.89). HMT denoising increased A_z from 0.89 to 0.90. The performance for online processing[3] is $A_z = 0.91 \pm 0.03$, where performance is measured by predicting the classification of the next sample using only past data.

III. Correcting Errors Using the Detected ERN

Using the detected ERN to correct human response errors requires choosing a threshold on the output of the linear classifier so as to minimize the number of errors $E_{\rm HM}$ made by the combined human–machine system. This is the number of errors E_H made by the subject alone, minus the number of those errors detected by our BCI system, *plus* the number of correct responses by the subject that were incorrectly classified as errors by our BCI system. Denote by $f_{\rm TE}$ the fraction of subject errors detected by the BCI system (true errors), and by $f_{\rm FE}$ the fraction of correct subject responses incorrectly classified as errors by our BCI system (false errors). We can write $E_{\rm HM} = E_H(1 - f_{\rm TE}) + C_H f_{\rm FE}$. However, $1 - f_{\rm TE} = f_{\rm FC}$, the fraction of subject errors that were incorrectly classified as correct responses (false correct). The number of human–machine errors is, therefore, $E_H f_{\rm FC} + C_H f_{\rm FE}$, which is the total number of classifier errors.

If we construct a classifier that estimates the class probability, we minimize the number of errors by assigning new trials to the class with the highest probability under the classifier. In terms of the log-odds-ratio, we minimize the error rate by choosing a threshold of zero. Since we employ Gaussian models with equal covariance matrices for the class distributions, the log-odds ratio is a linear function of the input. However, if the actual class distributions do not fit our model distributions, our linear discriminator is only an approximation to the true log-odds ratio, and the optimal threshold may differ from zero. This appears to be the case for this set of experiments, as we see in Fig. 5.

In our online implementation, we choose an optimal threshold by keeping a record of the outputs of the linear discriminator for the last 100 trials of both correct and erroneous responses. We then search for the threshold that minimizes the error rate on these sets, i.e., $E_H f_{\rm FC} + C_H f_{\rm FE}$. We estimate $f_{\rm FC}$ and $f_{\rm FE}$ from the outputs we have saved, and keep count of E_H and C_H from the trials we have seen thus far. The threshold is applied to a new sample that is not part of this training set. Table I summarizes the results for each subject. An experiment consists of about 600 button push responses of which 5%–20% are incorrect. The middle column show the error rate before correction. The average relative reduction in error rate for 7 subjects under online processing is $21.4\% \pm 21.7\%$. Note the large variance indicates very large improvements for some subjects and no improvement or slight degradations in performance for other subjects.

TABLE I
Summary of On-Line Error Correction for Each of Seven Subjects

Subject ID	original error rate in %	% error reduction[a]
3_27	6	23
3_30	10	-6
4_03	15	-1
4_04	15	49
4_05	13	27
4_09	14	47
4_10	18	12

[a]Negative values indicate degradation in performance.

In practical applications, the error correction system will not have access to the correct response. The parameters for the linear classifier and the detection threshold must be derived from an initial training sequence and are kept constant during operation. The performance numbers reported here reflect this scenario in that we report classification performance on the current trial using a classifier that is trained only on information from previous trials.

IV. Conclusion

We have described a set of linear preprocessing and classification algorithms for providing an accurate single-trial estimate of the ERN, an EEG signal which has been found to correlate with perceived error. The goal of measuring the ERN is to monitor a subject's task specific error rate and adapt an HCI to maximize overall performance. We have shown initial results for both offline and online correction of subject errors for an alternative forced choice visual discrimination task. Future work will investigate generalization of the approach to other tasks, particularly those which require more complex adaption of the HCI.

[3]The online version does not yet include the HMT denoising.

REFERENCES

[1] A. Kramer and J. Spinks, "Capacity views of information processing," in *Psychophysiology of Human Information Processing: An Integration of Central and Autonomic Nervous System Approaches*, R. Jennings and M. Coles, Eds. New York: Wiley, 1991, pp. 179–250.

[2] J. Beatty, "Task-evoked pupillary responses, processing load, and the structure of processing resources," *Psych. Bull.*, pp. 276–292, 1982.

[3] A. Gevins, M. Smith, L. McEvoy, H. Leong, and J. Le, "Electroencephalographic imaging of higher brain function," in *Philosophical Transactions of the Royal Society*, ser. B London, U.K., 1999, vol. 354, pp. 1125–1134.

[4] C. Tallon-Baudry, O. Bertrand, F. Peronnet, and J. Pernier, "Induced gamma-band activity during the delay of a visual short-term memory task in humans," *J. Neurosci.*, no. 11, pp. 4244–4254, 1998.

[5] F. Babiloni *et al.*, "Linear classification of low-resolution eeg patterns produced by imagined hand movements," *IEEE Trans. Rehab. Eng.*, vol. 8, pp. 186–188, June 2000.

[6] W. H. R. Miltner, C. H. Braun, and M. G. H. Coles, "Event-related brain potentials following incorrect feedback in a time estimation task: Evidence for a generic neural system for error detection," *J. Cog. Neurosci.*, pp. 788–798, 1997.

[7] S. Thorpe, D. Fize, and C. Marlot, "Speed of processing in the human viusal system," *Nature*, pp. 520–522, 1996.

[8] L. Parra, C. Alvino, A. C. Tang, B. A. Pearlmutter, N. Yeung, A. Osman, and P. Sajda, "Linear spatial integration for single trial detection in encephalography," *NeuroImage*, to be published.

[9] M. Falkenstein, J. Hoorman, S. Christ, and J. Hohnsbein, "ERP components on reaction errors and their functional significance: A tutorial," *Biolog. Psych.*, vol. 52, pp. 87–107, 2000.

[10] G. Schalk, J. Wolpaw, D. McFarland, and G. Pfurtscheller, "EEG-based communication: Presence of an error potential," *Clin. Neurophysiol.*, vol. 111, pp. 2138–2144, 2000.

[11] P. Sajda, A. Gerson, and L. Parra, "High-throughput image search via single-trial event detection in a rapid serial visual presentation task," in *Proc. 1st Int. IEEE EMBS Conf. Neural Engineering*, Capri, Italy, Mar. 2003.

[12] J. C. Woestenburg, M. N. Verbaten, and J. L. Slangen, "The removal of the eye-movement artefact from the EEG by regression analysis in the frequency domain," *Biolog. Psych.*, vol. 16, no. 1–2, pp. 127–147, 1983.

[13] T.-P. Jung, S. Makeig, C. Humphries, T.-W. Lee, M. J. Mckeown, V. Iragui, and T. J. Sejnowski, "Removing electroencephalographic artifacts by blind source separation," *Psychophysiol.*, vol. 37, pp. 163–178, 2000.

[14] M. S. Crouse, R. D. Nowak, and R. G. Baraniuk, "Wavelet-based statistical signal processing using hidden Markov models," *IEEE Trans. Signal Processing*, vol. 46, pp. 886–902, Apr. 1998.

[15] H. Coi and R. G. Baraniuk, "Multiscale imaage segmentation using wavelet-domain hidden markov models," *IEEE Trans. Image Processing*, vol. 10, pp. 1309–1321, Sept. 2001.

[16] H. Cheng and C. A. Bouman, "Multiscale bayesian segmentation using a trainable context model," *IEEE Trans. Image Processing*, vol. 10, pp. 511–525, Apr. 2001.

[17] J. K. Romberg, H. Coi, and R. G. Baraniuk, "Bayesian tree-stuctured image modeling using wavelet domain hidden markov models," *IEEE Trans. Image Processing*, vol. 10, pp. 1056–1068, July 2001.

[18] C. D. Spence, L. Parra, and P. Sajda, "Detection, synthesis and compression in mammographic image analysis using a hierarchical image probability model," in *Mathematical Methods in Biomedical Image Analysis*, M. Staib, Ed. Piscataway, NJ: IEEE Press, 2001, pp. 3–10.

[19] L. Rabiner, "A tutorial on hidden markov models and selected applications in speech recognition," *Proc. IEEE*, vol. 77, pp. 257–285, Feb. 1989.

Graz-BCI: State of the Art and Clinical Applications

G. Pfurtscheller, C. Neuper, G. R. Müller, B. Obermaier, G. Krausz, A. Schlögl, R. Scherer, B. Graimann, C. Keinrath, D. Skliris, M. Wörtz, G. Supp, and C. Schrank

***Abstract*—The Graz-brain–computer interface (BCI) is a cue-based system using the imagery of motor action as the appropriate mental task. Relevant clinical applications of BCI-based systems for control of a virtual keyboard device and operations of a hand orthosis are reported. Additionally, it is demonstrated how information transfer rates of 17 b/min can be acquired by real time classification of oscillatory activity.**

***Index Terms*—Brain–computer interface (BCI), event-related desynchronization/synchronization (ERD/ERS), motor imagery, rehabilitation, sensorimotor rhythms, virtual keyboard.**

I. INTRODUCTION

Currently available brain–computer interfaces (BCIs) can be grouped according to the kind of brain signals they process or the mode of operation they depend on. Within brain signals, we can, for example, differentiate between evoked potentials (EPs), slow cortical potential shifts, and oscillatory electroencephalogram (EEG) components. There are two main categories of mode-of-operation implemented by BCI systems. Within the first category, brain signals are analyzed in cue- or stimulus-triggered time windows either by identifying changes in EPs [1] and slow cortical potentials shifts [2], or quantifying oscillatory EEG components [3], [4]. These types of BCIs, operating with predefined time windows, are generally gathered under the term "cue-based" or "synchronous" BCI systems. Within the second category, a continuous analysis of brain signals is performed either with the purpose of detecting event-related potentials or transient changes in oscillatory EEG components. This type of BCI operates in an asynchronous mode. These are "noncue-based" or "asynchronous" BCI systems and, therefore, have been referred to as "asynchronous detectors" in as much as they operate on the basis of movement-related potentials [5], [6].

In the last decade, work on the Graz-BCI has focused predominately on characterizing and differentiating two or more brain states or EEG patterns, respectively, associated with motor imagery in predefined time windows (cue-based or synchronous BCI). Our research has been focused on methods of parameter estimation and on testing a considerable number of classifiers [7]–[9]. The currently implemented discrimination method is capable of differentiating between two brain states associated, in our case, with two different types of motor imagery in defined time windows. It can achieve classification accuracies from 80% up to 100% [4]. The neurophysiological basis for the Graz-BCI is the fact that actual performance of a limb movement and the imagination of the same movement activates similar cortical areas, as abundantly demonstrated by functional magnetic resonance imaging (fMRI) [10] and positron emission tomography (PET) investigations [11]. Similarly, the quantification of sensorimotor rhythms has shown that the spatiotemporal patterns of event-related

Manuscript received August 2, 2002; revised April 25, 2003. This work was supported in part by the Austrian Federal Ministry of Transport, Innovation, and Technology under project GZ140.587/2, the "Allgemeine Unfallversicherungsanstalt" (AUVA), and in part by the rehabilitation centers in Tobelbad (A) and in Bad Kreuznach (D, kreuznacher diakonie).

The authors are with the Department of Medical Informatics, Institute of Biomedical Engineering, University of Technology Graz, 8010 Graz, Austria, (e-mail: pfurtscheller@tugraz.at).

Digital Object Identifier 10.1109/TNSRE.2003.814454

1534-4320/03$17.00 © 2003 IEEE